DYNAMIC BEHAVIOUR OF THE L-H TRANSITION IN ASDEX-UPGRADE

H. Zohm,
ASDEX-Upgrade Team, ICRH-, NI-Group

IPP 1/276 September 1993

MAX-PLANCK-INSTITUT FÜR PLASMAPHYSIK

85748 GARCHING BEI MÜNCHEN

MAX-PLANCK-INSTITUT FÜR PLASMAPHYSIK

GARCHING BEI MÜNCHEN

DYNAMIC BEHAVIOUR OF THE L-H TRANSITION IN ASDEX-UPGRADE

H. Zohm,
ASDEX-Upgrade Team, ICRH-, NI-Group

IPP 1/276 September 1993

Die nachstehende Arbeit wurde im Rahmen des Vertrages zwischen dem Max-Planck-Institut für Plasmaphysik und der Europäischen Atomgemeinschaft über die Zusammenarbeit auf dem Gebiete der Plasmaphysik durchgeführt.

Dynamic Behaviour of the L-H Transition in ASDEX Upgrade

H. Zohm,
ASDEX-Upgrade Team, NI-, ICRH-Group
Max-Planck-Institut für Plasmaphysik,
D-85748 Garching, FRG, EURATOM-Association

Abstract - *The dynamic behaviour of the L-H transition in ASDEX-Upgrade is described. We focus on the periodic L-H-L transitions known as 'dithering H-mode' and show that there is an intrinsic timescale in this process which is characteristic for the L-H transition. We give a tentative explanation for the phenomenon using an extension of Itoh's model [1] for the L-H transition and find that this simple bifurcation model can qualitatively explain many of the experimental observations. According to our model, the dithering cycles are a limit cycle oscillation due to a difference in the response of the system to a rise in either T or n. The implications for H-mode theories are discussed.*

1. Introduction

The H-mode [2] is one of the most promising regimes of enhanced confinement for future large fusion devices. Although progress has been made in characterizing and understanding of the L-H transition [3], the physics of the process is not yet fully resolved. The aim of this paper is to show that bifurcation models for the L-H transition can be tested against experimental results by applying them to the dynamic behaviour of the L-H transition. In section 2, we summarize the experimental results from ASDEX-Upgrade. Section 3 describes the model we use. Results from modelling are presented in section 4. In section 5, a discussion of the results is given. Finally, section 6 presents our conclusions.

2. Experimental Results

The L-H transition occurs when the heating power P exceeds a given threshold P_{thr}. The threshold increases linearly with $n_e B_t$ and seems to be related to the power flux across the plasma edge [4]. In various tokamaks, at the power threshold, a sequence of L-H-L transitions is observed prior to the final transition into the H-mode. This phenomenon is known as 'dithering H-mode'. In the following, we will experimentally characterize this phase on the ASDEX Upgrade tokamak and compare the observations to a theoretical model.

The number of dithering cycles to appear at the transition varies with the rise of power flux into the plasma at the transition. Fig. 1 and 2 show two examples from ASDEX-Upgrade (note the different time axis !). Both shots are run in the lower single-null configuration with the ion ∇B drift towards the X-point (i.e. 'favourable drift direction') with $a = 0.5$ m, $R = 1.65$ m, elongation $\kappa = 1.6$ and Deuterium as the working gas. In the first case ($B_t = -2$ T, $I_p = 1.2$ MA, $\bar{n}_e = 5 \times 10^{19}$ m^{-3}, $P_{thr} \approx 2$

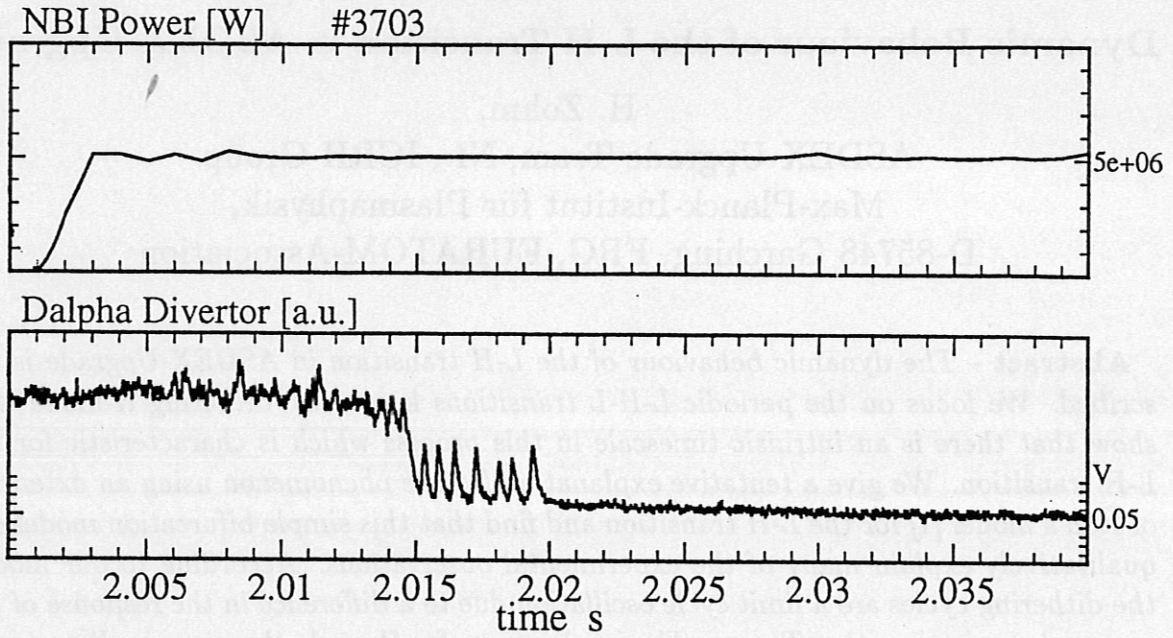

Figure 1: L-H transition with a steep rise of heating power ($\dot{P}_{exc} \approx (50\ \mathrm{ms})^{-1}$). Only 7 dithering cycles can be seen on the D_α trace

MW), NBI heating (H^0) of 5 MW is applied in a step function. The absorption of power in the plasma is governed by the slowing down time of the fast ions which is typically of the order of 10-20 ms. The flux from the core through the edge rises on the (longer) timescale of the global energy confinement time τ_E. In order to compare different cases, we therefore characterize them by the normalized rise of power in excess to the threshold divided by the rise time or, if longer, by τ_E:

$$\dot{P}_{exc} = \frac{1}{P_{thr}} \frac{d}{dt}(P - P_{thr}) \tag{1}$$

As $\tau_E \approx 120$ ms for the case shown, we have $\dot{P}_{exc} \approx (50\ \mathrm{ms})^{-1}$. With this fast ramp rate, few cycles appear. The opposite case is the ICRH heated discharge ($B_t = -2$ T, $I_p = 0.6$ MA, $\bar{n}_e = 3 \times 10^{19}\ \mathrm{m}^{-3}$, $P_{thr} \approx 1.2$ MW, D(H) minority heating) shown in Fig. 2. Here $\dot{P}_{exc} \approx (1\ \mathrm{s})^{-1}$ and dithering cycles are seen for 100 ms.

In the limit of $\dot{P}_{exc} \to 0$, which eventually occurs in ohmic H-mode discharges [4], a series of dithering cycles of very regular frequency ($\approx 1 - 2$ kHz in ASDEX Upgrade at I_p=0.8 MA, B_t=-1.35 T) appears for the whole H-phase of 2-3 s (i.e. $\approx$ 6000 cycles!) as seen in Fig. 3. Long dithering phases (up to 100 ms) at heating power close to P_{thr} have also occurred using NBI, but, so far, the stationary dithering H-mode was only seen during OH-heating. The dithering cycles are sometimes also referred to as 'grassy ELMs', but, as has been shown on ASDEX [5], do not show the typical MHD signatures of type III ELMs (which also appear close to P_{thr}). In the dithering phase, confinement only marginally improves ($\approx$ 10% above L-mode); this also is a remarkable difference to ELMy discharges which typically show an improvement of 1.5-1.8 with respect to L-mode.

We have shown that the number of dithering cycles to appear depends on the ramp

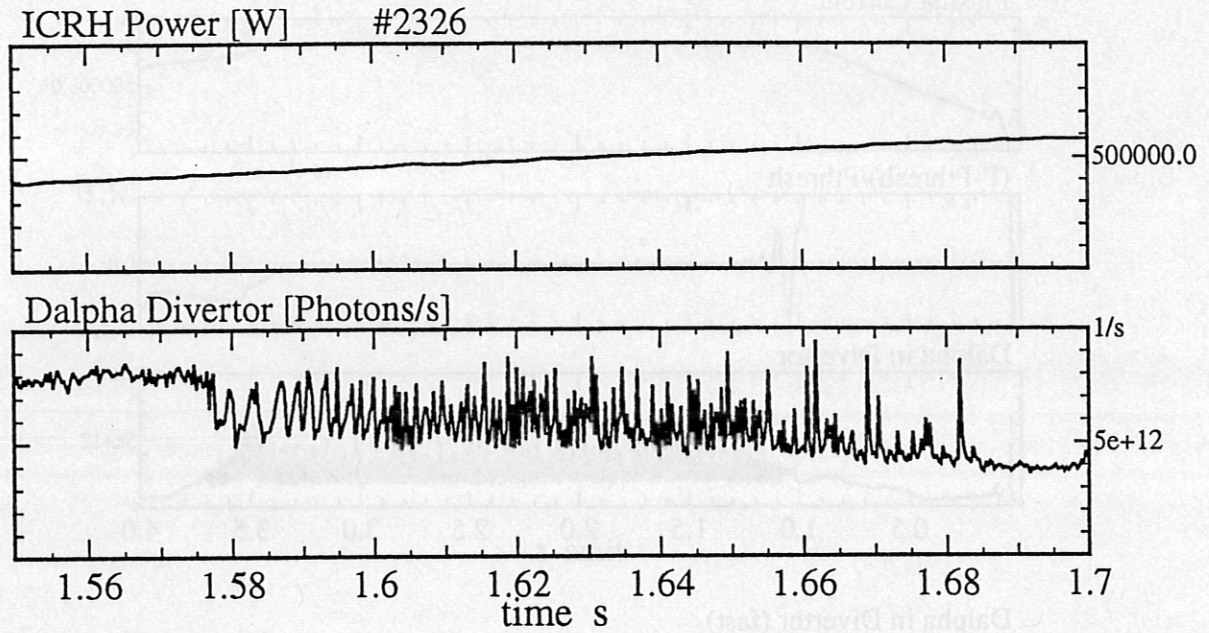

Figure 2: L-H transition with a slow rise of heating power ($\dot{P}_{exc} \approx (1\ \mathrm{s})^{-1}$). Dithering cycles are observed for ≈ 100 ms.

rate of the heating power in excess of P_{thr}. The frequency of the cycles, however, shows only a weak variation with plasma parameters or heating power and is roughly constant at 1-2 kHz. Only for shots with long dithering phases and a slow evolution towards the final H-mode transition, one can observe the frequency to vary by a factor of ≈ 2. This can be seen in the D_α trace of shot 2326 in Fig. 2. Note that during the temporal evolution, also the shape of the D_α signal varies. We will later give an interpretation of this phenomenon.

3. Theoretical Model

These experiments show that there is an intrinsic timescale in the L-H transition. In the following we will give a tentative explanation of this timescale and show how the various experimental results can be interpreted in terms of this approach. In order to model the dynamics of the L-H transition, we extend the model proposed in [1] based on a multivalued curve of the poloidal rotation or, in this approach equivalently, the radial electric field Z. The system was shown to exhibit so-called limit cycle oscillations, i.e. an oscillating solution between the static L- and H-mode regimes.

Transport equations are derived from mass conservation

$$\frac{\partial n}{\partial t} = -\nabla\vec{\Gamma} + S \tag{2}$$

where n is the particle density, $\vec{\Gamma}$ the particle flux and S a source term representing local sources (e.g. ionization). Energy conservation reads

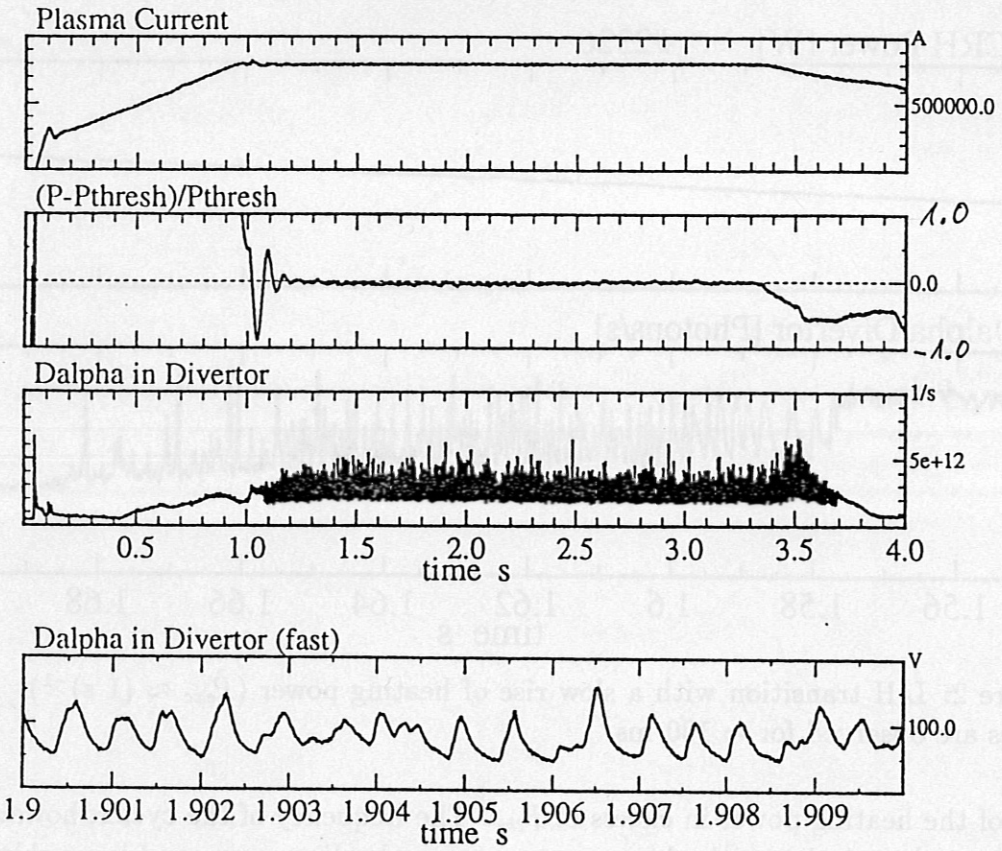

Figure 3: Steady state dithering cycles in an OH H-mode. The OH power is always marginal for the H-mode.

$$\frac{\partial}{\partial t}(\frac{3}{2}nT) = -\nabla\vec{q} + Q \tag{3}$$

where T is the temperature, $\vec{q}$ is the heat flux and Q represents a local energy source (e.g. ICRH heating). We make the following ansatz for the fluxes

$$\vec{\Gamma} = -D\nabla n \tag{4}$$

$$\vec{q} = -n\chi\nabla T + \frac{3}{2}T\vec{\Gamma} \tag{5}$$

where D is the particle diffusivity, χ the heat conductivity and we have not considered explicit drift velocities. Under the assumption $S = Q = 0$, i.e. no sources in the volume considered, the variation of density and temperature is then (in one dimension) given by

$$\frac{\partial n(x,t)}{\partial t} = \frac{\partial}{\partial x}\Big(D(Z(x,t))\frac{\partial n(x,t)}{\partial x}\Big) \tag{6}$$

$$\frac{\partial T(x,t)}{\partial t} = \frac{\partial}{\partial x}\Big(\frac{2}{3}\chi(Z(x,t))\frac{\partial T(x,t)}{\partial x}\Big) + \frac{1}{n}\Big(\frac{2}{3}\chi + D\Big)\frac{\partial n}{\partial x}\frac{\partial T}{\partial x} \tag{7}$$

The temporal evolution of the poloidal rotation or the radial electric field Z is given by

$$\frac{\partial Z(x,t)}{\partial t} = 0 = -N(Z,g) + \mu \frac{\partial^2 Z(x,t)}{\partial x^2} \tag{8}$$

$N(Z,g)$ is a nonlinear term that introduces the bifurcation:

$$N(Z,g) = g - g_1 + (\beta Z^3 - \alpha Z) \tag{9}$$

where the so-called gradient parameter g is given by [6]

$$g = const. \frac{1}{\rho_{p,i}\nu_i^*}\left(\frac{n'}{n} + \gamma\frac{T'}{T}\right) = g_0\frac{T}{n}\left(\frac{n'}{n} + \gamma\frac{T'}{T}\right) \tag{10}$$

The prime denotes the derivative with respect to x; g_0, g_1 and the Z-dependent term are chosen to analytically approximate the multivalued solution of poloidal rotation versus force [7] (or, as pointed out in [8], electric field against radial current) in the presence of a radial current (as is the case for electrode biasing experiments) or ion orbit losses and other mechanisms leading to a nonambipolar radial flux. This means that $Z(g)$ is single-valued for $g < g_L$ and $g > g_H$ whereas inbetween, three solutions of the cubic equation exist. Due to the symmetry of the cubic curve, the relation $(g-g_1)_L = -(g-g_1)_H$ holds. Fig 4 shows a typical curve $Z(g)$.

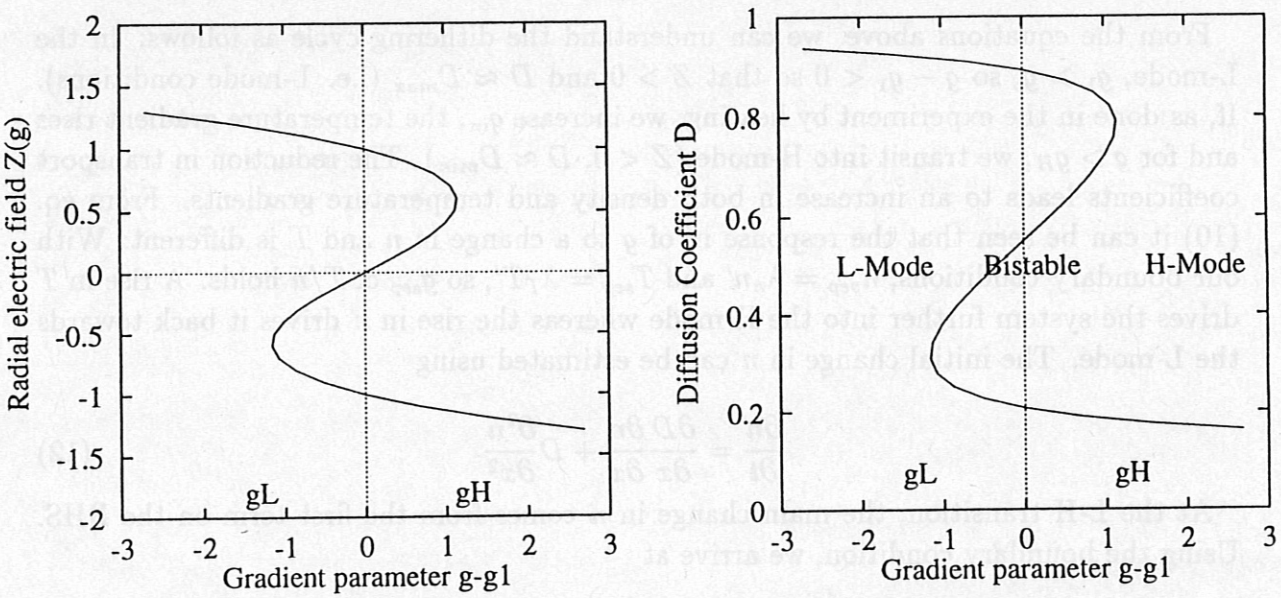

Figure 4: Model curve $Z(g)$ and $D(g)$.

The zero in eqn. (8) comes from the assumption that the profile of Z adjusts to changes in N on a much faster timescale than the plasma profiles and manages to keep the net radial current out of the plasma to zero. The coefficient μ is the differential viscosity between flux surfaces. Due to this term, the radial electric field cannot arbitrarily vary between neighbouring flux surfaces. For $\mu = 1$ m^2/s (which is of the order of experimental values [9]), the final profile $Z(x)$ is always a straight line.

The transport properties of the H-mode are modelled by

$$D(Z) = \frac{1}{2}(D_{max} + D_{min}) + \frac{1}{2}(D_{max} - D_{min}) \tanh Z \tag{11}$$

A similar equation is used for $\chi(Z)$. Here D_{max}, χ_{max} correspond to L-mode conditions and D_{min}, χ_{min} to the H-mode. A typical set we use is $D_{max} = 1$ m^2/s, $D_{min} = 0.1$ m^2/s and $\chi = 3D$. A model curve $D(g)$ is shown in Fig. 4.

Similar to [1], we find that a transport barrier, i.e. a zone where of radial extent Δ in which transport is reduced, develops for in the H-mode. The width Δ is governed by μ. The difference to [1] is that we include the temporal and spatial variation of the temperature; as will be shown below, this is a necessary ingredient to describe the experimental observations. We solve the equations (6), (7) and (8) simultaneously on a spatial domain extending over $\approx$ 2-3 poloidal ion gyroradii, i.e. from $x = 0$ at 2 cm inside the separatrix up to the separatrix. As has been shown [1], the radial extension of the domain does not influence the width of the transport barrier. The boundary conditions are $\Gamma_{in} = const.$ and $q_{in} = const.$ at the left boundary (representing the fluxes from the plasma core into the domain) and $1/(\lambda_n) = n'/n = const.$ and $1/(\lambda_T) = T'/T = const.$ at the separatrix. The boundary conditions for eq. (8) are $N(Z, g) = 0$ at both boundaries.

4. Modelling of Experimental Results

From the equations above, we can understand the dithering cycle as follows: In the L-mode, $g_1 > g$, so $g - g_1 < 0$ so that $Z > 0$ and $D \approx D_{max}$ (i.e. L-mode conditions). If, as done in the experiment by heating, we increase q_{in}, the temperature gradient rises and for $g > g_H$, we transit into H-mode ($Z < 0$, $D \approx D_{min}$). The reduction in transport coefficients leads to an increase in both density and temperature gradients. From eq. (10) it can be seen that the response in of g to a change in n and T is different: With our boundary conditions, $n_{sep} = \lambda_n n'$ and $T_{sep} = \lambda_T T'$, so $g_{sep} \propto T/n$ holds. A rise in T drives the system further into the H-mode whereas the rise in n drives it back towards the L-mode. The initial change in n can be estimated using

$$\frac{\partial n}{\partial t} = \frac{\partial D}{\partial x}\frac{\partial n}{\partial x} + D\frac{\partial^2 n}{\partial x^2} \tag{12}$$

At the L-H transition, the main change in n comes from the first term on the RHS. Using the boundary condition, we arrive at

$$\frac{1}{n_{sep}}\frac{\partial n_{sep}}{\partial t} \approx \frac{\partial D}{\partial x}\frac{1}{\lambda_n} \tag{13}$$

A similar equation can be derived for T_{sep}. The necessary condition for dithers to appear is $dg_{sep}/dt < 0$ after the transition. Replacing $\partial D/\partial x$ by $(D_{max} - D_{min})/\Delta$ and $\partial\chi/\partial x$ by $(\chi_{max} - \chi_{min})/\Delta$, where Δ is the typical width of the transport barrier, we arrive at the necessary condition for the dithering cycle

$$\frac{1}{\lambda_n}(D_{max} - D_{min}) > \frac{2}{3}\frac{1}{\lambda_T}(\chi_{max} - \chi_{min}) \tag{14}$$

(note that this is not a sufficient condition as g may decrease, but, depending on the choice of g_0 and g_1, never reach the value g_L where it transits to L-mode again). For small ramp rates of the heating power, dithers may be expected using experimental values [2] of $\lambda_n \approx 1$ cm, $\lambda_T \approx 3$ cm, χ and D as mentioned above. If g decreases below g_L, the system will go back to L-mode, then decrease the density gradient and go into the H-mode again. This happens until the heating (increase in q_{in}) finally overcomes the decrease in g due to the steepening of the density gradient and the system stays in H-mode.

In order to correctly describe the dynamics of the cycle, we have to consider another timescale: Once the barrier is established, the first term of the RHS of eqn. (12) vanishes and normal diffusion (second term on the RHS) becomes dominant. The rise in n is now governed by

$$n(t) = n_L + (n_H - n_L)(1 - e^{-\frac{t}{\tau_n}}) \tag{15}$$

where $\tau_n \approx \Delta^2/D_{min}$ is the diffusion time in the barrier and the values n_L, n_H are the steady state edge values in H-mode or L-mode: in steady state, $\Gamma_{in} = \Gamma_{out}$ and

$$n_{sep} = \Gamma_{in}\lambda_n/D_{sep} \tag{16}$$

It is this timescale that governs the evolution of g after the initial jump introduced by the change in D. Similar equations hold for the response of T to the jump in χ.

The timescale of the dithering cycle is thus given by the time it takes to change the gradients in the transport barrier region. In our simulations, this is typically a width of ≤ 1 cm at a diffusion coefficient in between 0.1 and 1 m^2/s. From this, a typical timescale of 1-10 kHz results which is in the range of the experimental observation.

We now consider the effect of the heating power: The ramp in q_{in} leads to a continuous rise in T and drives g into the region $g > g_H$ i.e. into stationary H-mode. If the temperature rise rate is small compared to the frequency of the dithering cycles, lots of dithers are observed, for a fast rise, only few dithers appear. This explains why the number of cycles depends on the power ramp rate as shown in Fig. 1 and 2. Fig. 5 shows the temporal evolution of the gradient parameter and the power flux out of the plasma obtained from modelling for two different ramp rates.

With a slow rise in heating power we are also able to reproduce the experimental observation of the shape of the D_α trace. An example from the modelling is shown in Fig. 6: At the first L-H transition, g decreases quickly from g_H to g_L, in the subsequent transitions, this timescale gets slower and slower. The reason for this is a difference of the temporal evolution of n and T due to eqn. (15). For $t/\tau_n \ll 1$, the rate of change of n is given by

$$\dot{n}/n_L \approx (n_H/n_L - 1)/\tau_n \tag{17}$$

with a similar equation for T. During the cycle, T rises due to the change in q_{in}. With each cycle, the steady state values increase: $T_H \rightarrow T_H^*$, $T_L \rightarrow T_L^*$ where the * denotes the value in the next cycle. As T_H and T_L are increased by the same factor ($\propto q_{in}$), we find $T_H/T_L = T_H^*/T_L^*$, and the relative rise in T is always the same. On the other hand,

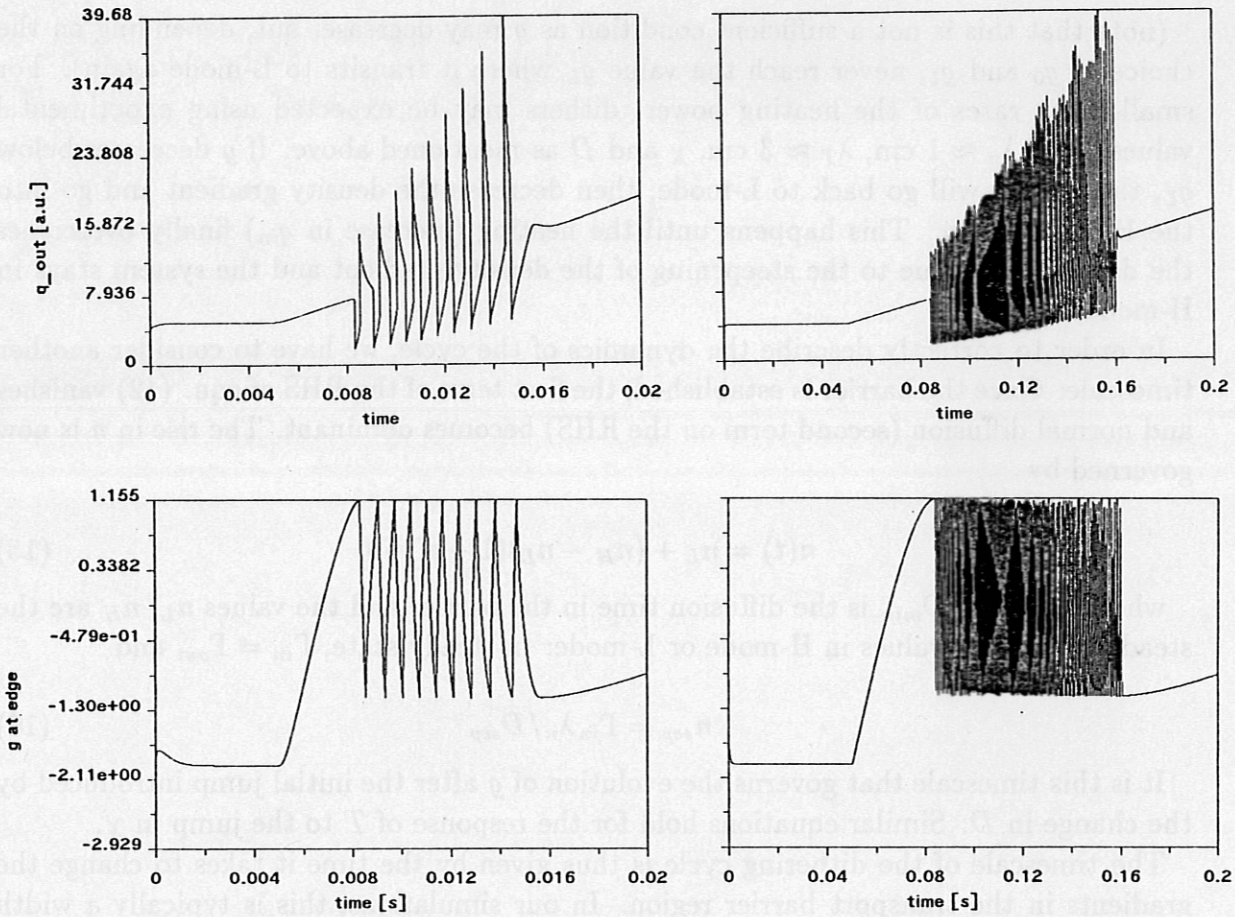

Figure 5: Temporal evolution of q_{out}, the power flux at the separatrix, and $g - g_1$, the gradient parameter, in response to different ramp rates of q_{in}. Left: Ramp from L- to H-mode in 10 ms, right: Ramp from L- to H-mode in 100 ms. Note the different time axis.

the increase in T means, that at g_H, $n_L^* > n_L$ holds (remember $g_H \propto T/n = const.$). On the other hand, there is no increase in n_H ($\Gamma_{in} = const$); this means $n_H^*/n_L^* < n_H/n_L$ and the relative rise of n gets smaller until finally, $g > g_L$ is always fulfilled. The change in the rise rate of n leads to the observed change in the signal shapes allowing for longer and longer H-mode phases.

5. Discussion

We have shown that, with a simple bifurcation model, we can reproduce the experimental signatures of the dynamics of the L-H transition. For this, we used the numbers g_0 and g_1 as free parameters. These two parameters determine the width of the bistable region of the gradient parameter g. Thereby, the frequency of the dithering cycles is determined. In our modelling, we chose g_0 and g_1 in order to match the experimentally observed frequency. In this parameter regime, the timescale of the dithering cycle is determined by diffusion across the width of the transport barrier rather than by the

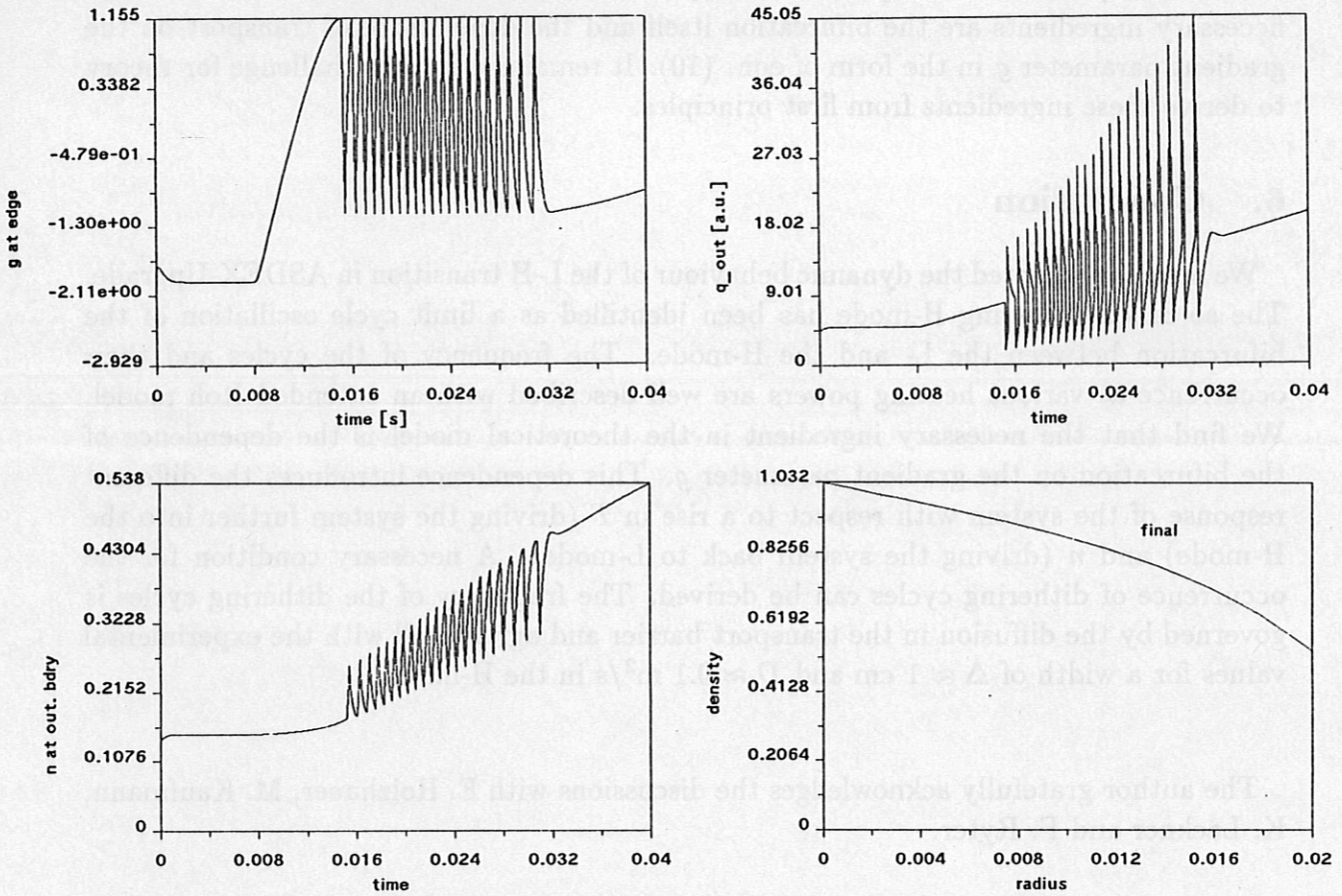

Figure 6: Results from modelling: Temporal evolution of the gradient parameter $g - g_1$, energy flux q_{out} and density at the separatrix. Also shown is a final (H-mode) density profile.

magnitude of the jump in the transport coefficients at the transition. No attempt was made to compare our values of g_0 and g_1 to existing theories; this remains a further issue for a more detailled study.

In order to correctly include the physics of the L-H transition, the following points may be subject to further discussion: While the modelling of the heating power as a flux from the core is a reasonable assumption, this is different for the particle flux: The particle sources in the edge region are not negligible and their dependence on the plasma parameters, especially at the L-H transition, might lead to changes in the dynamical behaviour of the system. Also, the change in edge parameters at the transition might influence the loss of fast particles from the edge, thereby changing the shape and/or extension of the bifurcation curve. Finally, we have not included a specific transport model; it is now widely believed that the reduction of fluctuations in the edge is responsible for the improvement of D and χ, however, this effect should rather be governed by the shear in the radial electric field than by the value of Z itself. Also, in our model, the reduction in transport appears instantaneously after the system has reached the $g = g_H$. Here, physics understanding of the process might introduce a new timescale. However, the fact

that our simplified model reproduces many of the experimental results shows that the necessary ingredients are the bifurcation itself and the dependence of transport on the gradient parameter g in the form of eqn. (10). It remains a further challenge for theory to derive these ingredients from first principles.

6. Conclusion

We have investigated the dynamic behaviour of the L-H transition in ASDEX-Upgrade. The so-called dithering H-mode has been identified as a limit cycle oscillation of the bifurcation between the L- and the H-mode. The frequency of the cycles and their occurrence at various heating powers are well described with an extended Itoh model. We find that the necessary ingredient in the theoretical model is the dependence of the bifurcation on the gradient parameter g. This dependence introduces the different response of the system with respect to a rise in T (driving the system further into the H-mode) and n (driving the system back to L-mode). A necessary condition for the occurrence of dithering cycles can be derived. The frequency of the dithering cycles is governed by the diffusion in the transport barrier and agrees well with the experimental values for a width of $\Delta \approx 1$ cm and $D \approx 0.1$ m^2/s in the H-mode.

The author gratefully acknowledges the discussions with E. Holzhauer, M. Kaufmann, K. Lackner and F. Ryter.

References

[1] S. Itoh, K. Itoh, A. Fukuyama, and Y. Miura, Phys. Rev. Lett. **67**, 2485 (1991).

[2] The ASDEX Team, Nucl. Fusion **29**, 1959 (1989).

[3] K. H. Burrell et al., Plasma Phys. Controlled Fusion **34**, 1859 (1992).

[4] F. Ryter et al., Controlled Fusion and Plasma Physics, Proceedings of the 20th European Conference, Lisbon **I**, 10 (1993).

[5] H. Zohm et al., Nucl. Fusion **32**, 489 (1992).

[6] S. Itoh and K. Itoh, Phys. Rev. Lett. **60**, 2276 (1988).

[7] K. C. Shaing and E. C. Crume, Phys. Rev. Lett. **63**, 2369 (1989).

[8] T. Stringer, An explanation of the L to H transition induced by applied radial voltage, Technical Report JET-P(93)07, JET Joint Undertaking, 1993.

[9] A. Kallenbach et al., Nucl. Fusion **30**, 645 (1990).